Biosensors and Bioelectronics 142 (2019) 111501

Contents lists available at ScienceDirect

Biosensors and Bioelectronics

journal homepage: www.elsevier.com/locate/bios

High resolution monitoring of chemotherapeutic agent potency in cancer cells using a CMOS capacitance biosensor

Bathiya Senevirathna[a,b], Sheung Lu[a,b], Marc Dandin[c], John Basile[d], Elisabeth Smela[e], Pamela Abshire[a,b,*]

[a] Department of Electrical and Computer Engineering, University of Maryland, College Park, MD, USA
[b] Institute for Systems Research, University of Maryland, College Park, MD, USA
[c] Department of Electrical and Computer Engineering, Carnegie Mellon University, Pittsburgh, PA, USA
[d] Department of Oncology and Diagnostic Sciences, University of Maryland School of Dentistry, Baltimore, MD, USA
[e] Department of Mechanical Engineering, University of Maryland, College Park, MD, USA

ARTICLE INFO

Keywords:
CMOS capacitance biosensor
Drug screening
Cancer cell cytotoxicity
Lab-on-chip

ABSTRACT

Monitoring cell viability and proliferation in real-time provides a more comprehensive picture of the changes cells undergo during their lifecycle than can be achieved using traditional end-point assays. Particularly for drug screening applications, high-temporal resolution cell viability data could inform decisions on drug application protocols that might lead to better treatment outcomes. We describe a CMOS biosensor that monitors cell viability through high-resolution capacitance measurements of cell adhesion quality. The system consists of a $3 \times 3\,mm^2$ chip with an array of 16 sensors, on-chip digitization, and serial data output that can be interfaced with inexpensive off-the-shelf components. An imaging system was developed to provide ground-truth data of cell coverage concurrently with data recordings. Results showed the sensor's ability to detect single-cell binding events, track cell morphology changes, and monitor cell motility. A chemotherapeutic assay was conducted to examine dose-dependent cytotoxic effects on drug-resistant and drug-sensitive cancer cell lines. Concentrations higher than 5 μM elicited cytotoxic effects on both cell lines, while a dose of 1 μM allowed discrimination of the two cell types. The system demonstrates the use of real-time capacitance measurements as a proof-of-concept tool that has potential to hasten the drug development process.

1. Introduction

Cell-based assays can analyze the effects of different materials and growth conditions on cells cultured *in vitro*. They are a vital tool in the drug discovery process and can be used to quantify the cytotoxic effects of drugs. Most cell-based screening studies require the use of specialized laboratory equipment and reagents, and they provide data through methods that require labeling such as fluorescent, bioluminescent, or colorometric staining. While these screens can provide high-throughput analysis through parallelization of experiments, they generally have high operational costs, can be labor intensive, require sub-sampling of analytes, and may lack specificity (Méry et al., 2017). Furthermore, most provide data at temporally and spatially sparse sampling points or are endpoint assays requiring cell fixation, and so do not provide information on the dynamics of live cell growth and motility.

Real-time monitoring of cell viability over the course of drug exposure and subsequent cell death may provide a more complete picture of the cytostatic and cytotoxic effects of drugs. In particular, profiling cancer cell responses with high-temporal resolution can provide insight into cell death kinetics enabling the development of more beneficial drug dosage regimens and better-targeted therapies (Forcina et al., 2017; Wolbers et al., 2004; Wolpaw et al., 2011). Indeed modern chemotherapeutic regimens generally involve the use of multiple drugs (Frei and Eder, 2003) administered sequentially or in alternation, with the aim of reducing drug resistance, reducing non-specific toxic effects, and maximizing overall efficacy. Computational models have been developed to generate adaptive therapeutic regimes (Gatenby et al., 2009) or select optimum strategies to address issues of tumor heterogeneity (Zhao et al., 2014). Therefore the ability to perform continuous cell measurements in real-time represents a significant advance over current methods of determining drug cytotoxicity and cancer cell susceptibility; replacing current assays with a more rapid and more

* Corresponding author. 2211 A.V. Williams Building, 8223 Paint Branch Dr., College Park, MD, 20742, USA.
E-mail addresses: bsenevir@umd.edu (B. Senevirathna), sheunglu@umd.edu (S. Lu), mdandin@andrew.cmu.edu (M. Dandin), jbasile@umaryland.edu (J. Basile), smela@umd.edu (E. Smela), pabshire@umd.edu (P. Abshire).

https://doi.org/10.1016/j.bios.2019.111501
Received 8 May 2019; Received in revised form 8 July 2019; Accepted 12 July 2019
Available online 13 July 2019
0956-5663/

relevant alternative could hasten the drug development process toward clinical implementation.

Complementary metal-oxide semiconductor (CMOS) technology has been leveraged to develop biosensors to meet this goal by bringing sensing and signal processing electronics into intimate contact with biology. This has the advantages of incorporating the signal transduction and readout pipeline into a single highly integrated platform, thus enabling miniaturization and high-fidelity measurements. Among the different possible sensing modalities for CMOS technologies, impedance and capacitance-based sensors have shown promise in cell viability monitoring. These sensors operate by monitoring the capacitive loading of cells at the cell-chip interface (Hong et al., 2011; Prakash and Abshire, 2005). Several such platforms have been developed for detecting bacterial cells (Couniot et al., 2016), monitoring bacterial growth (Ghafar-Zadeh et al., 2010), and tracking cancer cell proliferation (Laborde et al., 2015; Nabovati et al., 2017; Prakash and Abshire, 2008). A recent study looked at drug screening on chip using a capacitance sensor (Nabovati et al., 2019), comparing cells that were antibiotic-resistant with those that were non-resistant. Results showed a positive correlation with expected outcomes, although the temporal resolution of measurements was on the order of hours, which may limit the ability to observe drug-induced responses over short timespans. Other CMOS sensing modalities have also been studied for drug development, including electrical sensing of action potential variations upon drug dosing (Abbott et al., 2017; Lopez et al., 2018; Park et al., 2018).

In this work, a CMOS-based capacitance biosensor is presented that enables automatic, real-time, and label-free cell tracking to monitor chemotherapeutic agent potency. The device is able to generate measurements of cell-substrate coupling with high spatial, temporal, and amplitude resolution, which in turn can be used to monitor cell adhesion, proliferation, and viability in the presence of a cytotoxic agent. Prior work has presented sensor characterization results and preliminary live cell experiments (Senevirathna et al., 2019, 2018). Here, more comprehensive cell experiments are performed with the addition of time-lapse optical imaging of the sensor surface to verify measurements. This ground-truth validation confirms the operation of the chip and its ability to detect single-cell binding and detachment events. Furthermore, experiments were performed to use the biosensor as a proof-of-concept drug-screening tool. Two human ovarian cancer cell lines were grown on the device, one of which is sensitive to a chemotherapeutic agent and the other resistant. Repeated experiments were performed to monitor cell viability for different concentrations of the drug, and results demonstrate the ability to discriminate the resistant and sensitive cell lines through capacitance measurements. The high-temporal resolution measurements were then used, along with mathematical modeling, to estimate kinetics of cell death by measuring the time lag between drug exposure and death onset, and the rate of cell death. Results showed that cell death is induced faster with increased drug concentration, while the death rate remains unaffected. Capacitance and image data may be found online at http://dx.doi.org/10.21227/9zzd-w936 (Senevirathna et al., IEEE Dataport, 2019).

2. Materials and methods

2.1. Sensor design & theory

2.1.1. Cell-substrate coupling & chemotherapy

The CMOS biosensor operates by monitoring capacitive changes that occur at the cell-substrate interface as cells settle onto a substrate, adhere, proliferate, and eventually lift off due to cell death, forced detachment, or other morphological changes. Fig. 1a shows a diagram of three stages of the cell adhesion process. When cells are first placed in suspension they drift downwards and make an initial attachment with the substrate (top panel, Fig. 1a and b). They then begin attaching to the surface through a variety of cell adhesion mechanisms (middle panel, Fig. 1a and b) (Lodish et al., 2000). The cells then anchor and flatten themselves, spreading outward over a larger area until they reach their maximum spread (bottom panel, Fig. 1a and b) (Khalili and Ahmad, 2015). Healthy cells will continue to bind tightly to the substrate and spread out as they grow and proliferate, while compromised cells contract and may even lift off from the surface entirely. These changes in cell morphology modulate the dielectric properties of the cell-substrate interface which can be measured as changes in surface capacitance (Prakash and Abshire, 2008). Therefore, by integrating highly sensitive capacitance sensors directly underneath the cells, one can obtain an accurate measure of cell health and viability.

2.1.2. CMOS capacitance biosensor

The biosensor platform consists of a CMOS microchip that measures capacitance directly at the cell-substrate interface, converts it to a digital signal, and sends data off-chip to a microcontroller readout board. The chip includes a 4×4 array of capacitance to frequency (CTF) sensors with a spatial pitch of $196 \times 186\ \mu m$. Fig. 1c shows a schematic of the sensing paradigm. Each sensing site consists of a pair of interdigitated electrodes covering an area of $30 \times 30\ \mu m^2$ that are fabricated in the top-metal layer of the CMOS process. This electrode configuration was chosen following finite element model simulations that showed increased capacitance sensitivity compared to planar electrodes (Senevirathna et al., 2016). These electrodes are separated from the cell culture area by a SiO_2/Si_3N_4 passivation layer.

As cells settle and adhere to the substrate, they modulate the capacitance sensed by the underlying circuitry. A detailed description of the basic sensor element design can be found in prior work (Senevirathna et al., 2018). Briefly, each sensing site consists of a voltage-controlled oscillator (VCO), as shown in the bottom-left of Fig. 1c, which generates an output voltage that switches between HIGH and LOW at a frequency governed by internal parasitic resistances and capacitances, and a fixed analog bias voltage (V_B). Here, the sensing electrodes are electrically connected across the stages of the VCO, thereby introducing an additional capacitive load (C_{IN}) which modulates the oscillation frequency (f_{IN}). The chip digitizes the frequency by integrating the oscillating signal through a shared counter for a fixed amount of time. On-chip control logic automatically activates each sensor in the array sequentially using row/column decoders that set each sensor's active-low enable signal ($\overline{EN}$). Data for each sensor is stored in local memory on-chip before being sent off-chip to a microcontroller through a two-wire I^2C serial communication interface. This interface was chosen to minimize wiring requirements and to facilitate chip packaging.

2.2. Sensor integration & data readout

The biosensor chip was fabricated in a commercial 3-metal 0.35 μm CMOS process. An image of the CMOS chip can be seen in Fig. 2a. The chip was packaged in biocompatible materials to make experimentation possible in the aqueous biological environment. Two different packaging methods were used. The first method involved encapsulating the die in an epoxy mold, patterning a zinc/copper/nickel metal stack to make electrical contacts with the chip, and finally passivating the electrical traces using a second layer of epoxy. Further details of the process can be found in (Lu et al., 2018). The second method involves mounting the chip to a low-temperature co-fired ceramic (LTCC) carrier by using Au–Au thermocompression bonding. Under-filling with epoxy was used to create a liquid tight seal between the sensor chip and the LTCC carrier. Further details of the process can be found in (Halonen et al., 2016; Kilpijärvi et al., 2018). For both packaging methods, cell culture wells were created by gluing either standard microbiology or polypropylene tubes around the sensing area. No variation in chip characteristics or performance were observed due to choice of packaging method.

The readout system consisted of two printed circuit boards (PCBs), a

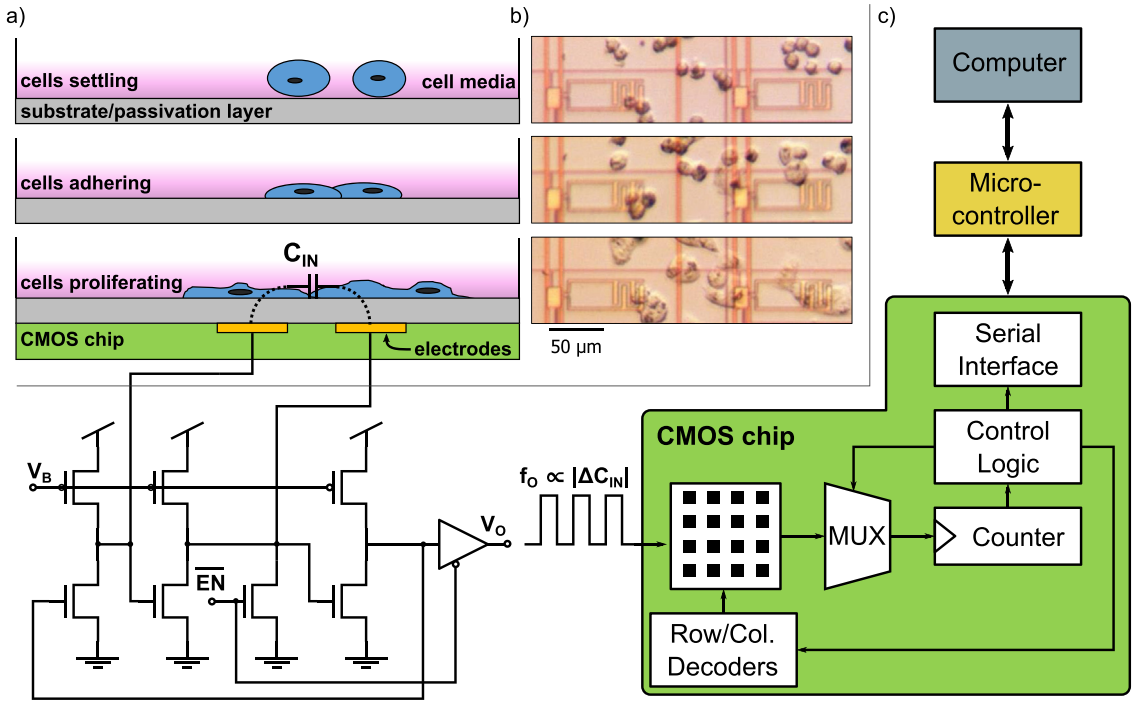

Fig. 1. The cell adhesion process and working principle of the capacitance biosensor. **a)** Cell dielectric layer formation on a solid substrate. Cells in suspension first drift downwards to settle on the surface. They begin adhering to the surface through various mechanisms involving cell adhesion molecules (Lodish et al., 2000). The cells then anchor and spread outward as they proliferate. **b)** Microscope images of cells cultured on the biosensor surface, during the settling, adhering, and proliferating phases (top to bottom). **c)** Schematic of the capacitive biosensor interfacing with the cell dielectric layer. Capacitive coupling of the cell layer through an insulation layer modulates the output frequency of a voltage-controlled ring oscillator. The frequency of the sensor output signal is proportional to the change in sensed capacitance. This information is digitized by integrating the signal through a counter. The resulting count value is then sent off-chip through a serial interface to a microcontroller and computer.

daughterboard that housed the chip and a motherboard that held the microcontroller (MicroPython PYB v1.0) used for readout. The daughterboard contained a zero-insertion-force socket that the chip plugged into. The motherboard contained headers that interfaced with the microcontroller. A flat shielded Ethernet cable was used to connect the two PCBs. The microcontroller stored the data locally on an SD card and also sent the data to a graphical user interface on a computer (custom MATLAB GUI) which plotted the data in real time.

2.3. Cell culture preparation

Human ovarian cancer cells, CP70 and A2780, were cultured in T25 flasks with growth media. The media consisted of RPMI 1640 serum (ThermoFisher Scientific) with 10% fetal bovine serum (ThermoFisher Scientific), and it was supplemented with 1% penicillin and streptomycin (ThermoFisher Scientific). The cells were grown in a standard T-cell flask within an incubator (37 °C, 5% CO_2) until they reached the log growth phase (Davis, 2011). Cells were detached from the flasks using 0.25% trypsin/EDTA (ThermoFisher Scientific), pelleted, and re-suspended into 12.5 mL of fresh cell media.

Cisplatin, a widely used platinum-based chemotherapeutic drug, was used as the anti-cancer agent. The agent was obtained in dry powder form (BioVision) and prepared with DI water to create a 1 mM stock solution. The solution was stored at room temperature away from light. For treatment, cells were plated into the device and allowed to grow for 48 h before the chemotherapeutic agent was applied.

Cell counting was performed using a hemocytometer and optical microscope. Counts were repeated in triplicate and averaged. For each experiment, a cell density of 10^5 cells/ml was used within the plating area of the device.

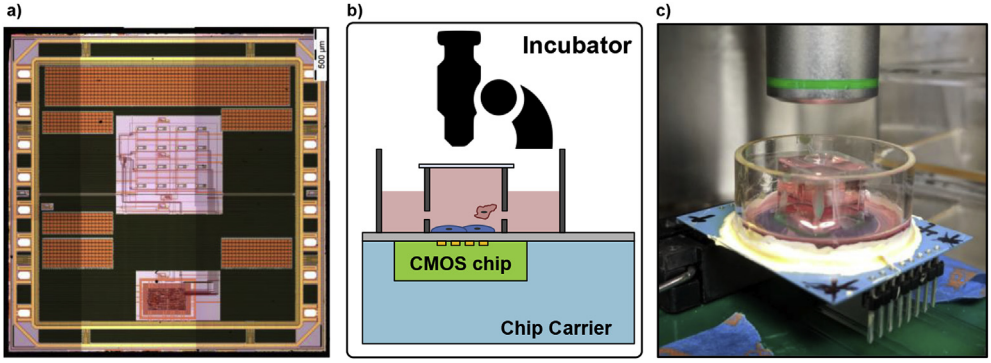

Fig. 2. The fabricated and assembled CMOS biosensor. a) Photomicrograph of the 3 × 3 mm^2 CMOS biosensor chip. **b)** Schematic and **c)** photograph of packaged chip surmounted by two-well combination.

2.4. Experimental setup

2.4.1. Sensor preparation

The packaged devices were prepared for experiments by first sterilizing them with UV light (30 min) in a hood and then rinsing them with deionized water, phosphate buffer solution (Dulbecco's Phosphate Buffer Solution), and cell media in sequence. Repeated experiments were conducted using the same device by following a cleaning protocol. The device was first rinsed with sterile water for several seconds and then an enzyme-activated detergent (Alconox Tergazyme, 1% solution) was added to the well. The solution was agitated using a plastic transfer pipette for several seconds before being left in the well for a further 15 min. The well was then rinsed for at least 5 min with sterile water.

2.4.2. Real-time imaging system

Optical microscopy, including phase-contrast and inverted light microscopy, is traditionally used to validate cell measurements by visual inspection. However, conventional imaging methods are generally incompatible with lab-on-CMOS devices since they require samples with substrates that are optically transparent. Since the sensor chips in lab-on-CMOS applications are opaque, traditional reflected light microscopy was used. Imaging of the sensor array was performed using a standard microscope head unit (Microzoom II, Bausch & Lomb) and microscope camera (MU1603, Amscope) in a custom-machined positioning assembly. The setup was designed to fit inside a standard cell culture incubator to allow for real-time imaging concurrently with data collection from the chip. This allowed for continuous imaging at high temporal resolution, compared with imaging on a bench outside the incubator, which would require interruption of experiments. Time-lapse imaging was automatically triggered every 5 min by the readout microcontroller to synchronize images with data readout.

Mammalian cells require cell media solution that matches physiological conditions and remains at a constant pH. This was achieved by maintaining a constant CO_2 level (5% in air) inside the incubator while allowing gas exchange with the media. This can lead to evaporation of cell media over time, which in turn causes loss of image focus. A two-well package was created to alleviate this issue, as shown in Fig. 2b. One well served as the area in which cells were cultured and imaging was performed. This well was within a larger secondary reservoir well that was left uncovered and allowed for gas exchange. The primary well was formed by gluing a cuvette around the exposed chip using a biocompatible silicone glue (Kwik-Cast, World Precision Instruments). The cuvette had 5 mm holes drilled through two sides at the bottom that served as ports to allow fluid exchange with the reservoir. Both wells were filled with cell culture media up to the height of the primary well, and a sterile glass coverslip was placed over the primary well. Cell media from the reservoir well was then aspirated out until the coverslip settled and formed a tight seal over the main well. An image of the setup is shown in Fig. 2c. Through this two well approach, physiological pH was maintained in the media through gas exchange in the reservoir well, and constant image focus was maintained through fixed focal distance in the main well.

3. Results & discussion

3.1. Correlation of cell adhesion and capacitance measurements

In order to validate the capacitance sensor measurements, experiments were first conducted with the imaging and sensor recordings running concurrently. Fig. 3 shows time-lapse images taken using the in-incubator imaging system along with the corresponding capacitance measurements for four sensors in the array. A video of the images and data with alignment markers can be found in Supplementary Materials (SV1). During this portion of the experiment, cells were pipetted into the culture well over the sensor array, then allowed to settle onto the chip surface in a random manner. As cells first seeded onto the surface they were rounded, as can be seen in image A of Fig. 3. While this initial binding is weak, a noticeable difference was seen in channels 2 and 4, which had an initial seeding of cells compared to channels 1 and 3, which were void of cells. Over the next several hours, the cells began to flatten and adhere more strongly, as can be seen in the progression to images B and then C. Corresponding capacitance increases to 380 aF and 600 aF were seen in channels 2 and 4, respectively. Channel 3 showed a brief increase in capacitance between hours 19 (image D) and 22 (image E). This was due to the cell on the top-right of the electrode, which traversed from the top of the electrode to the bottom over this time period, briefly increasing the capacitive coupling. Additionally, channel 1 showed a sharp increase in capacitance of ~200 aF at 21 h. This was due to the cell to the top-right of its electrodes, which moved downwards towards the center of the electrodes and remained there, as can be seen between images D and E. Channel 2 measured a brief 215 aF dip in capacitance at 19 h. This was due to the cell on top of the electrodes (image C) undergoing cell division. The two resulting daughter cells (image D) covered approximately the same area of electrodes as the parent, but the daughter cells were probably not as well adhered, resulting in a drop in measured capacitance. Over the next several hours these cells started to grow and to bind to the substrate, resulting in the increase in measured capacitance.

The array consists of 16 sensor sites spanning an area of $618 \times 588\,\mu m^2$; this is a relatively low spatial density. Richer information about the cell growth cycle could be ascertained with a higher density array. However, increased density would introduce tradeoffs between spatial resolution, amplitude resolution, and sensor readout speed. As designed, the current chip reads out each pixel every 1.4 s, a choice that aimed to mitigate the effects of parasitics and improve sensor resolution (Senevirathna et al., 2016). A simple method of increasing sensor density while maintaining the same theoretical resolution would be to parallelize the readout mechanism. This is a low-cost approach since multiple counters can be used to integrate the sensor signals, in either a row-wise or column-wise fashion. Alternatively, groups of sensors could be activated/deactivated in an interactive fashion. This could be used to focus readouts into certain locations of the array, for example if no cells are observed in one location compared to another location.

Control of cell binding location is a challenge for experiments with lab-on-CMOS capacitance sensors due to the relatively small sensing area of the input electrodes. Cell loading in this work was performed by dispensing aliquots of cell solution using a micropipette. Once in solution, the cells randomly distributed themselves across the entire well area. One way to better control cell seeding location would be to use microfluidics. By fabricating channels over the sensing area of the chip, cells could be loaded onto specific areas of the substrate, unloaded for passaging, and exposed to other reagents (Lin et al., 2004).

3.2. Cell response to chemotherapeutic agents

The CMOS capacitance biosensor was used to monitor the viability of cells in the presence of cisplatin, a widely used chemotherapeutic agent. The two lines of human ovarian cancer cells were cultured as described in Section 2.3. The cells were allowed to grow and proliferate for at least 48 h before cisplatin was administered directly into the cell growth well. Fig. 4 shows exemplar images of cells on the sensor surface through a drug administration experiment. The left-most image, taken at $t = 26.8$ h, shows cells growing normally. A 100 μM dose of cisplatin was administered at $t = 53.5$ h, indicated by the red line, and the second image shows the surface 6 h later. Cells still appeared to be healthy although a downtrend in the measured binding capacitance can be observed in the sensor data traces. Roughly 4 h later, a more noticeable change in cell morphology can be seen, both in the images and data. Capacitance decreases of 230 aF and 440 aF were measured in channels 1 and 2, respectively. Images of the chip surface show that the cells appeared noticeably shrunken and rounded, which is indicative of

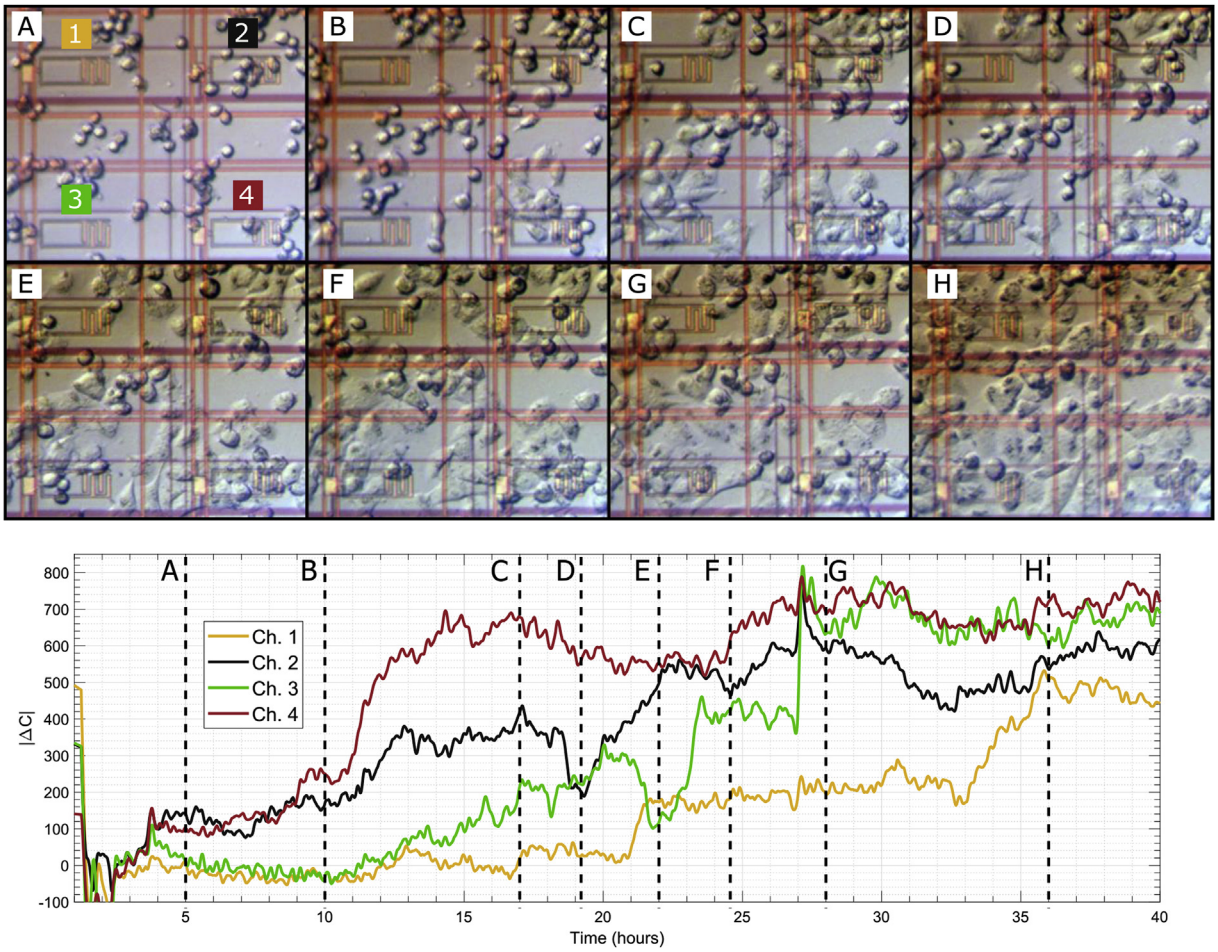

Fig. 3. Correlation of capacitance measurements and time-lapse imaging of cells on the chip during cell-substrate binding. Top: Images taken of four sensors at different time points. Time-lapse video is in Supplementary Materials (SV1). **Bottom**: Corresponding sensor responses showing the measured capacitance changes over time. The letter markers indicate the time points corresponding to each frame.

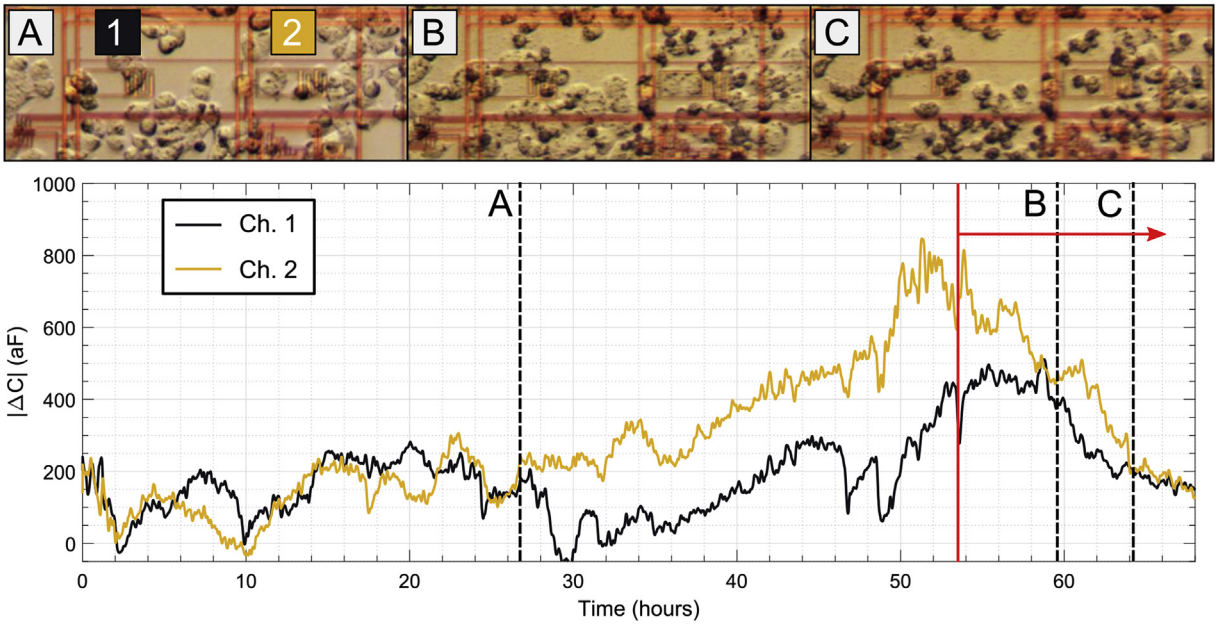

Fig. 4. Cisplatin-induced cell death can be measured using the capacitance biosensor. Top: Microscope images of the two sensors, 1 and 2, during a drug administration experiment. **Bottom:** Corresponding sensor-measured capacitance changes over time. The cisplatin was added at t = 53.5 h, indicated by the red line and arrow. The labels on the images correspond to the time points marked by the dashed vertical lines. Time-lapse video is in Supplementary Materials (SV2). (For interpretation of the references to color in this figure legend, the reader is referred to the Web version of this article.)

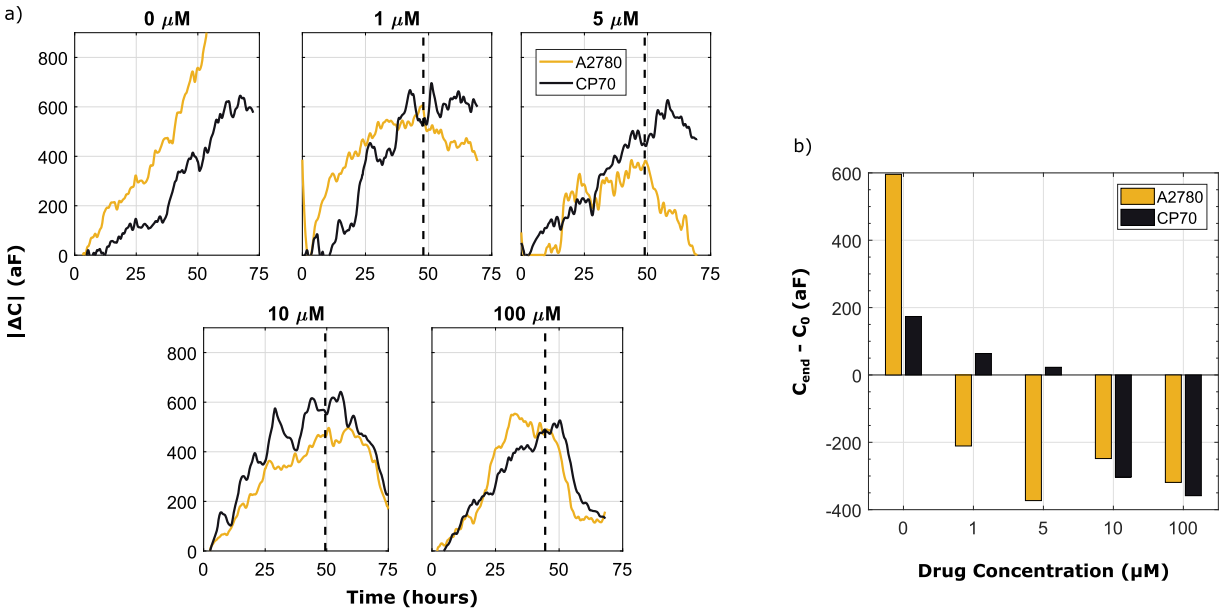

Fig. 5. Cisplatin induced cell death is drug concentration dependent. a) Mean capacitance sensor responses for various concentrations of applied drug (added after 2 days of growth). Each chart shows the response for two cell types, A2780 (drug-sensitive), and CP70 (drug-resistant). The dashed black line indicate when the drug was applied to the cell culture. In the control experiment both cell lines were viable through the experiment. Addition of 1 μM cisplatin showed an immediate effect on the capacitive coupling of A2780 cells while CP70 cells remained stable. Higher concentrations began to induce a response in CP70 cells as well. **b)** Measured difference in average capacitance from immediately after the drug was administered to 24 h afterwards.

cell death (Susan, 2007). Time-lapse video of cell death along with sensor measurements can be found in Supplementary Video SV2. This experiment shows the device's ability to track cell health in real time through a drug-screening experiment.

3.2.1. Dose responses

We then investigated dose-dependent effects of cisplatin on the two cell lines. Each cell type was allowed to grow for at least 48 h, after which different concentrations of cisplatin were applied. Control experiments were performed in which both cell lines were plated and allowed to proliferate unencumbered over the experimental period. Fig. 5a shows the time-series capacitance measurements of the device as a function of drug dose. Each trace shows the mean response of those sensors in the array that were visually observed to have cell coverage. Sensors that were void of cells, due to the random initial seeding, were omitted. The red and black lines correspond to the cisplatin-sensitive (A2780) and cisplatin-resistant (CP70) cell lines, respectively. The dashed black lines indicate the time at which the drug was administered.

The time-series data shows how drug dosage affected cell viability. As expected, the control experiment showed a continual increase in measured capacitance as cells proliferated without damage. At the same time, for high dosages, both cell lines were observed to be adversely affected. As drug concentration was reduced from 100 μM, the net effect diminished. At a concentration of 1 μM, the resistant CP70 line was seen to be relatively unaffected by the drug whereas the sensitive A2780 line showed a downtrend. This observation was confirmed by imaging the surface after the experiment was completed. The difference between the two responses can be highlighted by looking at the net change in measured capacitance at the time of drug application and 24 h later. The resulting change is shown in Fig. 5b. There was a net positive change in signal for the CP70 line for drug concentrations up to 5 μM, although the magnitude decreased with increasing concentration. At the same time, the A2780 line showed an immediate decrease in viability with a 1 μM cisplatin dosage. At concentrations of 10 μM and 100 μM, both cell lines were affected, as mentioned previously.

3.2.2. Cell death kinetics

We analyze the high-resolution data provided by the device to profile the temporal response of the cancer cells to cisplatin. The kinetics of cell death are characterized by the time delay between exposure to the drug and the onset of cell death (t_D), and the decay rate (r_D). The onset of cell death was extracted from the capacitance measurements by finding the time at which the peak capacitance value (C_D) occurs, after the application of the drug. The capacitance curves were then normalized to C_D and the data was fitted to an exponential decay model:

$$C(t) = \Delta C(t)/C_D = C_0 \exp(-r_D t) + C_B \quad (1)$$

where t (hr) is time, r_D is the exponential decay rate (hr^{-1}), C_0 and C_B are initial and baseline values, and $C(t)$ is the normalized capacitance as a function of time.

Cells were cultured as described previously and exposed to 25 and 100 μM dosages of cisplatin, concentrations that were previously confirmed to be lethal to both cell lines. Fig. 6a shows the normalized capacitance measurements of two sensors from experiments where A2780 and CP70 cell lines were exposed to 25 μM of cisplatin. For clarity, the measurements from the start of cell culture up to the time at which drug is administered are omitted. Additionally, the data is time-aligned such that the onset of cell death occurs at $t = 0$ h. Therefore t_D is the time span between the first data point and $t = 0$ h, as indicated by the horizontal arrows. Fig. 6b shows the corresponding plots for a dose level of 100 μM. The dashed lines in both figures are the fitted exponential decay models for each trace. Fig. 6c shows the mean t_D for each dosage and cell line. As can be seen, there is a significant decrease in the time to onset of cell death when drug dosage is increased from 25 to 100 μM ($p = 0.003$ and $p = 0.004$ for A2780 and CP70 cells, respectively). Fig. 6d shows the mean r_D values. No significant difference in the decay rate was seen as a function of drug concentration ($p > 0.05$). Interestingly, the rate of decay is higher for the resistant CP70 cell line compared to the sensitive A2780 line.

Drug delivery in these experiments involved dispensing microliter volumes of the drug into a relatively large well, so drug exposure relied primarily on diffusion through the cell media. As mentioned previously, microfluidics could be incorporated into future versions of the device in

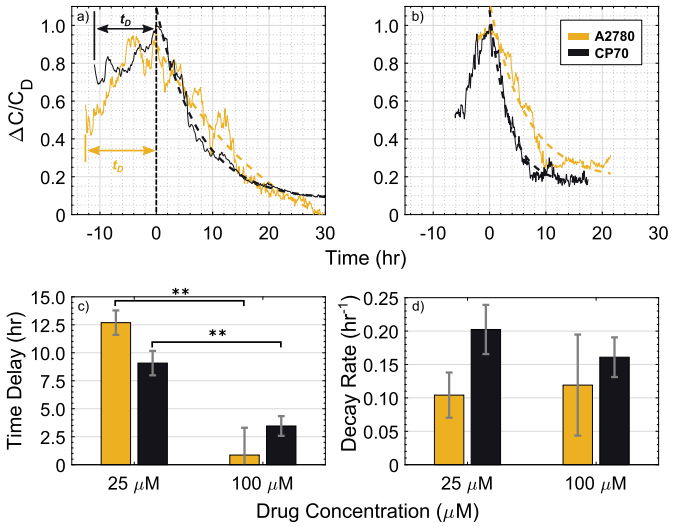

Fig. 6. Cell death kinetics. Normalized capacitance values vs. time for experiments where cells were exposed to drug concentrations of **a)** 25 μM and **b)** 100 μM. The bottom panel shows the mean extracted **c)** time delay and **d)** decay rate for the set of experiments. (**p < 0.01).

order to better control dosage. With channels running across the sensing area, one could precisely control flow rates to maintain a constant drug level. Additionally, exposure times could be controlled, allowing for evaluating different dosage regimens with multiple drug combinations. Furthermore, drug dispensing could be regulated by incorporating cell cycle marker detection, creating a feedback control loop for automated cell cycle-targeted drug screening therapies.

4. Conclusion

This paper presents a CMOS biosensor that monitors the potency of chemotherapeutic agents in cancer cells in real-time. The custom CMOS chip contains a 4 × 4 array of capacitance sensor pixels that make high-resolution measurements of cell-substrate coupling, as an indicator of cell adhesion and viability. The sensor was first validated by simultaneously acquiring capacitance measurements and time-lapse images of the sensor surface during *in vitro* experiments. Results showed strong evidence of the correlation between cell-substrate coupling and measured capacitance, and the ability of the sensor to monitor cells at the single-cell level, including cell division and movement events. Further experiments were performed to examine the effects of a chemotherapeutic agent on drug-sensitive and drug-resistant human ovarian cancer cell lines. Cell viability was tracked continuously over three days for a range of drug concentrations, and results showed the ability to successfully discriminate sensitive and resistant cell lines through capacitance measurements. The temporal responses of the measured capacitance to the chemotherapeutic agent were used to extract parameters of cell death kinetics, and showed that the time duration between exposure to the agent and onset of cell death is correlated with drug concentration.

The CMOS capacitance sensor used in this work has a relatively low spatial density of sensing sites, with 16 sets of input electrodes spread out over an area of 618 × 588 μm^2. The electrodes themselves are 30 × 30 μm^2 in size; therefore the actual sensing area is roughly 120 × 120 μm^2. Future studies will aim to overcome this limitation by increasing the number of sensing sites and reducing the spacing between electrodes, in order to create a high-density capacitance sensor array. Furthermore, microfluidics could be incorporated into the system to better control cell exposure to chemotherapeutic agents, as mentioned in Section 3.2.2. The capacitance sensor could then be used to explore cytotoxic effects to cells in a high-throughput manner. The drug administration profile could also be applied in a time-varying manner (e.g. pulsing or ramping) to investigate effects on cells that would not be possible with traditional laboratory-based cytotoxicity assays.

Declaration of competing interest

The authors declare that they have no known competing financial interests or personal relationships that could have appeared to influence the work reported in this paper.

Funding

This study was supported the ClintoxNP program (Project #268944) and UMD-UMB 2015 Research and Innovation Seed Grant Program.

CRediT authorship contribution statement

Bathiya Senevirathna: Software, Validation, Formal analysis, Investigation, Data curation, Writing - original draft, Writing - review & editing, Visualization. **Sheung Lu:** Investigation, Writing - original draft, Visualization. **Marc Dandin:** Resources, Writing - review & editing. **John Basile:** Resources, Writing - review & editing, Funding acquisition. **Elisabeth Smela:** Conceptualization, Methodology, Resources, Writing - review & editing, Supervision, Project administration, Funding acquisition. **Pamela Abshire:** Conceptualization, Methodology, Resources, Writing - original draft, Writing - review & editing, Supervision, Project administration, Funding acquisition.

Acknowledgements

The CMOS chip used in this study was designed at UMD with technical feedback from Joni Kilpijärvi, Niina Halonen, Antti Hassinen, Maciej Sobocinski, Jari Juuti, and Sakari Kellokumpu from the University of Oulu, Finland and from Anita Lloyd Spetz, Kalle Bunnfors, Kajsa Uvdal, and Natalia Abrikossova from Linköping University, Sweden. The LTCC Ceramic packaging of the chip was processed at the Microelectronic Research Unit, University of Oulu, Finland. The authors would like to thank Dr. Yan Shu from the University of Maryland Baltimore for providing the human ovarian cancer cells used in this study. The Center of Microscopy and Nanotechnology at the University of Oulu is acknowledged for technical support.

Appendix A. Supplementary data

Supplementary data to this article can be found online at https://doi.org/10.1016/j.bios.2019.111501.

References

Abbott, J., Ye, T., Qin, L., Jorgolli, M., Gertner, R.S., Ham, D., Park, H., 2017. CMOS nanoelectrode array for all-electrical intracellular electrophysiological imaging. Nat. Nanotechnol. 12, 460–466. https://doi.org/10.1038/nnano.2017.3.

Couniot, N., Francis, L.A., Flandre, D., 2016. A 16x16 CMOS capacitive biosensor array towards detection of single bacterial cell. IEEE Trans. Biomed. Circuits Syst. 10, 364–374.

Davis, J.M., 2011. Animal Cell Culture : Essential Methods. John Wiley & Sons, Incorporated, Hoboken, UNITED KINGDOM.

Forcina, G.C., Conlon, M., Wells, A., Cao, J.Y., Dixon, S.J., 2017. Systematic quantification of population cell death kinetics in mammalian cells. Cell Syst 4, 600–610. e6. https://doi.org/10.1016/j.cels.2017.05.002.

Frei, E.I., Eder, J., 2003. Combination Chemotherapy, sixth ed. BC Decker, Hamilton.

Gatenby, R.A., Silva, A.S., Gillies, R.J., Frieden, B.R., 2009. Adaptive therapy. Cancer Res. 69, 4894–4903. https://doi.org/10.1158/0008-5472.CAN-08-3658.

Ghafar-Zadeh, E., Sawan, M., Chodavarapu, V.P., Hosseini-Nia, T., 2010. Bacteria growth monitoring through a differential CMOS capacitive sensor. IEEE Trans. Biomed. Circuits Syst. 4, 232–238. https://doi.org/10.1109/TBCAS.2010.2048430.

Halonen, N., Kilpijärvi, J., Sobocinski, M., Datta-Chaudhuri, T., Hassinen, A., Prakash, S.B., Möller, P., Abshire, P., Kellokumpu, S., Spetz, A.L., 2016. Low temperature co-fired ceramic packaging of CMOS capacitive sensor chip towards cell viability monitoring. Beilstein J. Nanotechnol. 7, 1871–1877. https://doi.org/10.3762/BJNANO.7.179.

Hong, J., Kandasamy, K., Marimuthu, M., Choi, C.S., Kim, S., 2011. Electrical cell-substrate impedance sensing as a non-invasive tool for cancer cell study. Analyst 136, 237–245. https://doi.org/10.1039/c0an00560f.

Khalili, A.A., Ahmad, M.R., 2015. A Review of cell adhesion studies for biomedical and biological applications. Int. J. Mol. Sci. 16, 18149–18184. https://doi.org/10.3390/ijms160818149.

Kilpijärvi, J., Halonen, N., Sobocinski, M., Hassinen, A., Senevirathna, B., Uvdal, K., Abshire, P., Smela, E., Kellokumpu, S., Juuti, J., Lloyd Spetz, A., 2018. LTCC packaged ring oscillator based sensor for evaluation of cell proliferation. Sensors 18, 3346. https://doi.org/10.3390/s18103346.

Laborde, C., Pittino, F., Verhoeven, H.A., Lemay, S.G., Selmi, L., Jongsma, M.A., Widdershoven, F.P., 2015. Real-time imaging of microparticles and living cells with CMOS nanocapacitor arrays. Nat. Nanotechnol. 10, 791–795. https://doi.org/10.1038/nnano.2015.163.

Lin, R., Sabounchi, P., Lee, L.P., Hung, P.J., Lee, P.J., 2004. Continuous perfusion microfluidic cell culture array for high-throughput cell-based assays. Biotechnol. Bioeng. 89, 1–8. https://doi.org/10.1002/bit.20289.

Lodish, H., Berk, A., Zipursky, S.L., Matsudaira, P., Baltimore, D., Darnell, J.E., 2000. Molecular Cell Biology, fourth ed. W.H. Freeman, New York.

Lopez, C.M., Chun, H.S., Wang, S., Berti, L., Putzeys, J., Van Den Bulcke, C., Weijers, J.W., Firrincieli, A., Reumers, V., Braeken, D., Van Helleputte, N., 2018. A multimodal CMOS MEA for high-throughput intracellular action potential measurements and impedance spectroscopy in drug-screening applications. IEEE J. Solid State Circuits 53, 3076–3086. https://doi.org/10.1109/JSSC.2018.2863952.

Lu, S., Senevirathna, B., Dandin, M., Smela, E., Abshire, P., 2018. System integration of IC chips for lab-on-CMOS applications. 2018 IEEE Int. Symp. Circuits Syst. 2–6. https://doi.org/10.1109/ISCAS.2018.8351395.

Méry, B., Guy, J.-B., Vallard, A., Espenel, S., Ardail, D., Rodriguez-Lafrasse, C., Rancoule, C., Magné, N., 2017. In vitro cell death determination for drug discovery: a landscape review of real issues. J. Cell Death 10. https://doi.org/10.1177/1179670717691251.

Nabovati, G., Ghafar-zadeh, E., Letourneau, A., Sawan, M., 2017. Towards high throughput cell growth screening: a new CMOS 8 x 8 biosensor array for life science applications. IEEE Trans. Biomed. Circuits Syst. 11, 380–391.

Nabovati, G., Ghafar-Zadeh, E., Letourneau, A., Sawan, M., 2019. Smart cell culture monitoring and drug test platform using CMOS capacitive sensor array. IEEE Trans. Biomed. Eng. 66. https://doi.org/10.1109/TBME.2018.2866830.

Park, J.S., Grijalva, S.I., Aziz, M.K., Chi, T., Li, S., Sayegh, M.N., Wang, A., Cho, H.C., Wang, H., 2018. Multi-parametric cell profiling with a CMOS quad-modality cellular interfacing array for label-free fully automated drug screening. Lab Chip 18, 3037–3050. https://doi.org/10.1039/c8lc00156a.

Prakash, S.B., Abshire, P., 2008. Tracking cancer cell proliferation on a CMOS capacitance sensor chip. Biosens. Bioelectron. 23, 1449–1457. https://doi.org/10.1016/j.bios.2007.12.015.

Prakash, S.B., Abshire, P., 2005. A CMOS capacitance sensor that monitors cell viability. IEEE Sensors 1177–1180. 2005. https://doi.org/10.1109/ICSENS.2005.1597915.

Senevirathna, B., Castro, A., Dandin, M., Smela, E., Abshire, P., 2016. Lab-on-CMOS capacitance sensor array for real- time cell viability measurements with I2C readout. IEEE Int. Symp. Circuits Syst. 2863–2866.

Senevirathna, B.P., Lu, S., Dandin, M.P., Basile, J., Smela, E., Abshire, P.A., 2018. Real-time measurements of cell proliferation using a lab-on-CMOS capacitance sensor array. IEEE Trans. Biomed. Circuits Syst. 12, 510–520. https://doi.org/10.1109/TBCAS.2018.2821060.

Senevirathna, B.P., Lu, S., Dandin, M.P., Smela, E., Abshire, P.A., 2019. Correlation of capacitance and microscopy measurements using image processing for a lab-on-CMOS microsystem. IEEE Trans. Biomed. Circuits Syst. https://doi.org/10.1109/TBCAS.2019.2926836.

Senevirathna, B.P., Lu, S., Dandin, M.P., Basile, J., Smela, E., Abshire, P.A., 2019. Measurements of cancer cell proliferation using a Lab-on-CMOS capacitance sensor with time-lapse imaging. IEEE Dataport. https://doi.org/10.21227/9zzd-w936.

Susan, E., 2007. Apoptosis: a reveiw of programmed cell death. Toxicol. Pathol. 35, 496–516. https://doi.org/10.1080/01926230701320337.

Wolbers, F., Buijtenhuijs, P., Haanen, C., Vermes, I., 2004. Apoptotic cell death kinetics in vitro depend on the cell types and the inducers used. Apoptosis 9, 385–392. https://doi.org/10.1023/B:APPT.0000025816.16399.7a.

Wolpaw, A.J., Shimada, K., Skouta, R., Welsch, M.E., Akavia, U.D., Pe'er, D., Shaik, F., Bulinski, J.C., Stockwell, B.R., 2011. Modulatory profiling identifies mechanisms of small molecule-induced cell death. Proc. Natl. Acad. Sci. 108, E771–E780. https://doi.org/10.1073/pnas.1106149108.

Zhao, B., Hemann, M.T., Lauffenburger, D.A., 2014. Intratumor heterogeneity alters most effective drugs in designed combinations. Proc. Natl. Acad. Sci. 111, 10773–10778. https://doi.org/10.1073/pnas.1323934111.